

# NavFormer: A Transformer Architecture for Robot Target-Driven Navigation in Unknown and Dynamic Environments

Haitong Wang, Aaron Hao Tan, *Student Member, IEEE* and Goldie Nejat, *Member, IEEE*

**Abstract**—In unknown cluttered and dynamic environments such as disaster scenes, mobile robots need to perform target-driven navigation in order to find people or objects of interest, while being solely guided by images of the targets. In this paper, we introduce NavFormer, a novel end-to-end transformer architecture developed for robot target-driven navigation in unknown and dynamic environments. NavFormer leverages the strengths of both 1) transformers for sequential data processing and 2) self-supervised learning (SSL) for visual representation to reason about spatial layouts and to perform collision-avoidance in dynamic settings. The architecture uniquely combines dual-visual encoders consisting of a static encoder for extracting invariant environment features for spatial reasoning, and a general encoder for dynamic obstacle avoidance. The primary robot navigation task is decomposed into two sub-tasks for training: single robot exploration and multi-robot collision avoidance. We perform cross-task training to enable the transfer of learned skills to the complex primary navigation task without the need for task-specific fine-tuning. Simulated experiments demonstrate that NavFormer can effectively navigate a mobile robot in diverse unknown environments, outperforming existing state-of-the-art methods in terms of success rate and success weighted by (normalized inverse) path length. Furthermore, a comprehensive ablation study is performed to evaluate the impact of the main design choices of the structure and training of NavFormer, further validating their effectiveness in the overall system.

**Index Terms**—Dynamic and unknown environments, image-guided search, target-driven robot navigation.

## I. INTRODUCTION

Mobile robots can be used to search for potential victims in unknown environments including in urban disaster environments [1], [2], [3], in buildings engulfed by fire [4], and/or in collapsed mines [5]. Images of potential victims can be provided to the robots in order for them to search a disaster environment for these specific individuals, while avoiding collisions with rescue workers, victims, and other robots. In this paper, we address the problem of robot target-driven navigation (TDN) in unknown and dynamic environments. This problem requires a mobile robot to navigate an unknown and dynamic environment using only an onboard RGB camera to search for a static target given its image.

This work was supported in part by the Natural Sciences and Engineering Research Council of Canada (NSERC), and in part by the Canada Research Chairs program (CRC). (*Corresponding author: Haitong Wang.*)

The authors are with the Autonomous Systems and Biomechatronics Laboratory (ASBLab), Department of Mechanical and Industrial Engineering, University of Toronto, Toronto, ON M5S 3G8, Canada (e-mail: haitong.wang@mail.utoronto.ca; aaronhao.tan@utoronto.ca; nejat@mie.utoronto.ca).

TDN in unknown and dynamic environments is a challenging problem as: 1) there are no global maps of the environment available, therefore, a robot needs to reason about the spatial layout of the environment based on its own partial observations to prevent deadlocks and redundant coverage [6], and 2) the presence of dynamic obstacles needs to be detected for collision avoidance [7] and for spatial reasoning of the environment [8].

To-date, existing robot TDN methods for unknown environments have mainly used: 1) deep reinforcement learning (DRL) [6], [9], [10], or 2) imitation learning (IL) [11]. Images of targets have consisted of either indoor scenes (e.g., kitchen, bedroom) [9] or household objects (e.g., chair, microwave) [10]. These methods take RGB images as observations and the target image as input into a convolutional neural network (CNN) to extract features (e.g., geometry, patterns) and encode them into a latent vector. Namely, for DRL methods, navigation actions are generated using either fully connected layers (FCL) [9], long short term memory (LSTM) [10], or attention-based memory retrieval [6] approaches. For IL methods [11], a next expected observation (NEO) is predicted using a generative neural network. The robot action is then generated using an inverse dynamics model. These aforementioned TDN methods have mainly been applied to static environments. However, in dynamic environments, they may result in degraded performance due to the presence of moving obstacles that are treated as static. This may lead to misinterpretation of the spatial layout of the environment [8], which in turn can result in ineffective navigation decisions.

In this paper, we propose NavFormer, a novel end-to-end DL architecture consisting of a dual-visual encoder module and a transformer-based navigation network to address *for the first time* the problem of TDN in unknown and dynamic environments. NavFormer utilizes a decoder-only transformer [12] to make navigation decisions conditioned on both the target image and robot trajectory history. To obtain high-quality datasets for navigation policy learning, we decompose the task of TDN in dynamic environments into two existing sub-tasks: single-robot exploration, and multi-robot collision avoidance. Our main contributions in this paper include: 1) the development of the first end-to-end DL approach for robot target-driven navigation in unknown dynamic environments; 2) the incorporation of a dual-visual encoder system to extract static and general (i.e., static and dynamic) features for reasoning the spatial layouts of environments and collision avoidance, which is trained using self-supervised learning (SSL); and 3) the development of a cross-task training strategy

to train NavFormer on the two subtasks of single robot exploration and multi-robot collision avoidance. By using a cross-task training strategy we aim to transfer both learned exploration and collision avoidance skills to the primary TDN task without the need for specific fine-tuning.

## II. RELATED WORKS

In general, robot navigation methods address: 1) point-goal tasks, where the goal location relative to a robot is known a priori [13], and 2) target-driven tasks, where a robot is only provided with an RGB image of the target that either depicts a specific object [10] or a local region inside the environment [9]. Herein, we discuss the pertinent literature on: 1) robot target-driven navigation in static unknown environments, and 2) robot navigation in dynamic environments.

### A. Robot Target-Driven Navigation in Static Unknown Environments

Previous work has mainly used: 1) deep reinforcement learning [6], [9], [10], or 2) imitation learning [11] to address TDN tasks. For example, in [9], an architecture consisting of a shared Siamese network and scene-specific layers was used for robot TDN in indoor environments. Both the target image and current robot observation were taken as inputs to generate embeddings using a pre-trained ResNet50 [14]. The Asynchronous Advantage Actor Critic (A3C) [15] was used to train the navigation policy, where the output robot navigation action was obtained using scene-specific FCLs.

In [10], an object localization network and a navigation network with LSTM [16] were used for robot navigation in 3D mazes. The object localization network used a Siamese CNN to generate a one-hot vector to locate the target object. The navigation network incorporated an LSTM to account for robot historical observations to improve the spatial understanding of the environment. It was trained using the Importance Weighted Actor-Learner Architecture (IMPALA) [17]. Domain Randomization [18] was used during training to enable generalization to unseen maze environments.

In [4], a memory-augmented DRL architecture was developed for robot navigation in indoor environments. A state-embedding network was trained in a self-supervised manner to embed historical observations into a memory buffer. The navigation network consisted of a Siamese CNN network and an LSTM network. An attention module was used to retrieve memory embeddings and combined them with the current observation and the target image to generate navigation actions.

In [11], an architecture consisting of a generative module and an action prediction module was presented for robot indoor navigation. The generative module used the target image and the current robot observation to generate the NEO. The NEO was then used by the action prediction module to predict the robot's action based on the difference between the NEO and the current observation via a feed-forward network. IL was used to learn to predict the NEO from expert demonstrations.

### B. Robot Navigation in Dynamic Environments

Robot navigation methods in dynamic environments can be categorized as: 1) classical methods [7], [19]-[22], or 2) learning-based methods [23]-[27]. The most commonly used classical methods include Velocity Obstacle (VO)-based methods [7], [19], [20], the Artificial Potential Field (APF) [21], and the Dynamic Window Approach (DWA) [22]. Learning-based methods include: 1) DRL methods [23]-[25], which learn a navigation strategy through repeated interactions with the environment, and 2) hybrid methods [26], [27] using both DRL and IL which learn through both repeated interactions and expert demonstrations.

#### 1) Classical Methods

In [7], the VO method was used for robot collision avoidance in 2D dynamic environments by generating a potential collision area for a robot and a nearby moving obstacle (e.g., another robot) based on their current states (i.e., velocities, positions, and sizes). VO then selected the robot velocity that did not intersect with the collision area. Reciprocal VO (RVO) was introduced in [19] to address issues in movement oscillation of VO by taking the average of a velocity outside the collision area and the robot's current velocity. The Non-Holonomic Optimal Reciprocal Collision Avoidance (NH-ORCA) approach [20] was developed to extend VO-based methods for robots with non-holonomic constraints. In [21], APF was developed for robot collision avoidance using virtual forces generated by obstacles and robot goal locations in 2D environments with both static and dynamic obstacles. DWA was developed in [22] for mobile robot collision avoidance in 2D environments. Namely, a velocity search space of a dynamic window was defined by reachable robot velocities. DWA then selected the velocity that maximized an objective function.

#### 2) Learning-based Methods

In [23], a multi-robot collision avoidance architecture that directly maps laser scans to robot velocities was developed for a 2D particle world. Laser scans were encoded into a latent vector using a CNN, which was then concatenated with the robot's goal position and current velocity to generate the robot's velocity for the next timestep. Proximal Policy Optimization (PPO) [28] and curriculum learning were used to learn the navigation policy. In [24], the architecture in [23] was extended by incorporating a Gated Recurrent Unit (GRU) [29] to account for historical observations to improve temporal reasoning in unknown dynamic environments. In [25], RL-RVO was used for multi-robot collision avoidance in a 2D particle world. A set of sequential VO [7] and RVO [19] vectors representing the states of nearby obstacles were provided to a Bidirectional GRU network [29] to generate a navigation velocity.

In [26], a Hybrid CPU/GPU A3C for Collision Avoidance with DRL (GA3C-CADRL) method was developed for multi-robot collision avoidance also for a 2D particle world. An LSTM was used to encode the spatial information of nearby obstacles into a hidden state vector. The goal position was concatenated with the hidden state vector to generate robot velocities using FCLs. GA3C-CADRL was trained using IL and then GA3C [30]. In [27], the Pathfinding via Reinforcement and Imitation Multi-Agent Learning (PRIMAL) was developed for

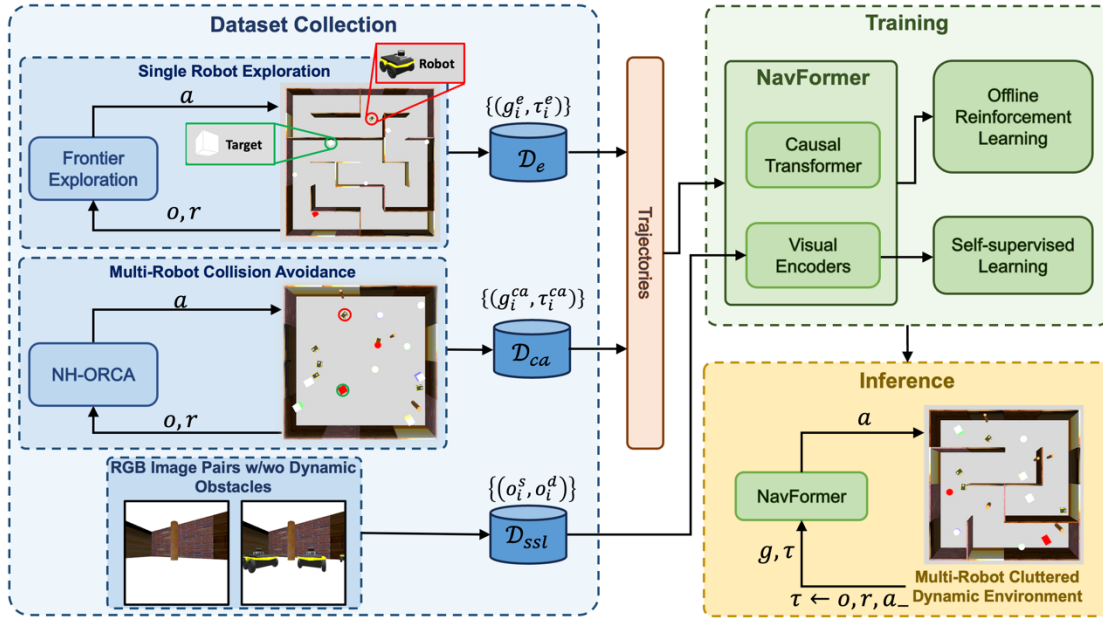


Fig. 1. NavFormer TDN architecture consisting of Dataset Collection, Training and Inference subsystems.

multi-robot navigation in 2D grid world environments. PRIMAL used a CNN to encode the local 2D map of static obstacles, nearby robots, and their goals into a latent vector. A LSTM network was then used to generate robot actions. During training, the PRIMAL framework randomly switched between DRL and IL to learn a navigation policy that achieved faster training and improved navigation performance.

### C. Summary of Limitations

The abovementioned target-driven methods [6], [9]-[11] address the problem of a single robot navigating to a target location in an unknown static environment. However, these methods do not consider dynamic obstacles such as other robots in their environments. This limitation may cause inaccuracies in spatial reasoning [8], potentially leading to degraded navigation performance.

Robot navigation in dynamic environments has been achieved using classical methods [7], [19]-[22], or learning-based methods [23]-[27]. These methods are reactive in that they consist of only local planning schemes without considering the global spatial layout of the environment. Therefore, a robot can become trapped in local minima (e.g., dead ends) in unknown environments [31]. Furthermore, they require the goal location to be a priori known and are not able to find a target provided in an RGB image without a given location. To address the above limitations, we have developed NavFormer, the first DL method for robot TDN in unknown and dynamic environments.

## III. TARGET-DRIVEN NAVIGATION PROBLEM IN UNKNOWN AND DYNAMIC ENVIRONMENTS

### A. Problem Definition

Robot target-driven navigation in unknown and dynamic environments describes the following problem: A mobile robot  $r$  needs to navigate to a target  $I$  utilizing only an RGB image of the target  $g$  and visual observations  $o \in \Omega$  (i.e., RGB images) of the environment obtained from an onboard camera.

The dynamic obstacles (i.e., other robots) in the environment are represented by a set  $M$ . There are no a priori global maps of the environment available and the 2D location of the static target object  $l_I$  is unknown. The target object is defined by a 3D geometric shape  $b \in B$  and color  $c \in C$ . The objective of the robot  $r$  is to minimize the expected travel distance  $d$  between the robot's start location  $l_s$  and target location  $l_I$ :

$$\min E[d(l_s, l_I)]. \quad (1)$$

### B. GC-POMDP for Robot Target-Driven Navigation

We model the robot TDN problem as a goal-conditioned partially observable Markov decision process (GC-POMDP) [32], [33]. GC-POMDP is described as a tuple  $(\mathcal{S}, \mathcal{g}, \mathcal{A}, \mathcal{P}, \mathcal{R}, \Omega, \mathcal{O})$ , where  $\mathcal{S}$  denotes the state space, and  $\mathcal{g}$  is the set of target RGB images. Robot actions,  $a \in \mathcal{A}$ , are represented by a 2D vector of linear and angular velocity.  $\mathcal{P}$  is the state transition function  $\mathcal{P}(s, a, s') = p(s'|s, a)$ .  $\mathcal{R}$  is the reward function,  $r = \mathcal{R}(s, a)$ .  $\Omega$  is the observation space and  $\mathcal{O}$  is the observation probability function  $\mathcal{O}(s', a, o) = p(o|s', a)$ . At each time step, the robot observes the environment, takes an action, then transitions to the next state and receives a reward.

The objective is to learn a policy  $\pi_\theta(a|g, \tau)$  that is conditioned on the target image  $g$  and robot historical trajectory  $\tau$  to maximize the expected return:  $E[\sum_{t=1}^T r_t]$ . The robot historical trajectory  $\tau$  consists of returns-to-go  $\hat{R}$ , observations  $o$ , and actions  $a$ :

$$\tau_t = (\hat{R}_1, o_1, a_1, \hat{R}_2, o_2, a_2, \dots, \hat{R}_t, o_t), \quad (2)$$

where the return-to-go is  $\hat{R}_t = \sum_{k=t}^T r_k$ , and represents the future desired return. The return-to-go at the first timestep,  $\hat{R}_1$ , is a user specified desired total rewards.

## IV. NAVFORMER ARCHITECTURE

The proposed NavFormer TDN architecture, Fig. 1, consists of three subsystems: 1) Dataset collection: to obtain datasets

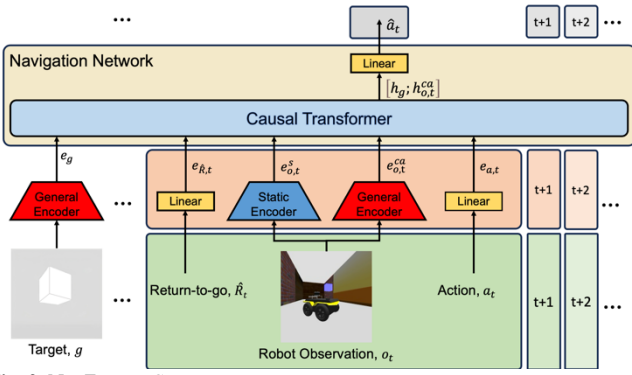


Fig. 2. NavFormer Structure.

containing robot trajectories for policy learning, and RGB image pairs for representation learning; 2) Training: to train both the NavFormer model using offline reinforcement learning and the dual-visual encoders using self-supervised learning, and 3) Inference: which implements the trained NavFormer model to perform TDN in unknown dynamic environments.

In this section, we will discuss the development of the NavFormer structure utilized by both the Training and Inference subsystems, Fig. 2. NavFormer contains: 1) a Multi-modal Input Sequence containing the target image  $g$  and robot trajectory  $\tau$ , 2) a Dual-visual encoder module that separately extracts static and general (i.e., static and dynamic) features from visual observations, and 3) a transformer-based Navigation Network that is conditioned on the embeddings of the multi-modal input sequence to generate navigation actions.

#### A. Multi-Modal Input Sequence

The multi-modal input sequence  $\mathcal{s}_t$  consists of the RGB image of the target  $g$  and robot trajectory  $\tau_t$ :

$$\mathcal{s}_t = (g, \hat{R}_1, o_1, a_1, \hat{R}_2, o_2, a_2, \dots, \hat{R}_t, o_t). \quad (3)$$

The sequence is converted to embeddings of the same dimension  $d_e = 128$ . We use a linear layer to project  $\hat{R}_i$  and  $a_i$  to embeddings  $e_{\hat{R},i}$  and  $e_{a,i}$ , respectively. These embeddings are combined with the embeddings output by the dual-visual encoders and provided to the Navigation Network.

#### B. Dual-Visual Encoders

NavFormer utilizes dual-visual encoders consisting of a static encoder  $f_s$  and a general encoder  $f_g$  to extract visual features from  $g$  and  $o$ . In particular,  $f_s$  extracts visual features only from static obstacles, which are used for spatial reasoning of the environment.  $f_g$  extracts visual features from both static and dynamic obstacles for collision avoidance.

Each encoder consists of a CNN with three convolutional layers with a kernel size, stride, and output channel of (8, 4, 32), (4, 2, 64), (3, 2, 64) [34]. All images (i.e.,  $g$  and  $o$ ) are in the dimension of (84, 84, 3). Given an input sequence  $\mathcal{s}_t$ ,  $g$  is used by  $f_g$  to generate a target embedding  $e_g$ . Furthermore, each observation  $o_i$  is used by  $f_s$  and  $f_g$  to generate a static embedding  $e_{o,i}^s$  and a general embedding  $e_{o,i}^{ca}$ , respectively.  $e_{o,i}^s$  and  $e_{o,i}^{ca}$  are then combined with the embedding of returns-to-go  $e_{\hat{R},i}$  and actions  $e_{a,i}$  from Section IV.A. Thus,  $\mathcal{s}_t$  is converted

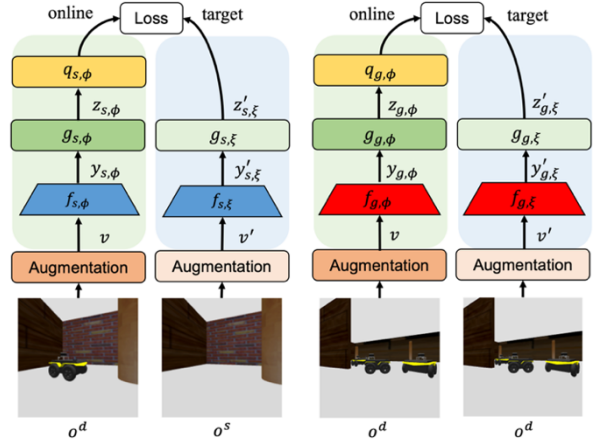


Fig. 3. BYOL procedure for the static and general encoder.

into a sequence of embeddings  $E_{s,t}$  which is then used by the Navigation Network to generate navigation actions:

$$E_{s,t} = (e_g, e_{\hat{R},1}, e_{o,1}^s, e_{o,1}^{ca}, e_{a,1}, \dots, e_{\hat{R},t}, e_{o,t}^s, e_{o,t}^{ca}). \quad (4)$$

#### 1) Training Loss

In order to train the two visual encoders, the Bootstrap Your Own Latent (BYOL) [35] self-supervised learning method is used. We use BYOL since it is a self-supervised learning technique that can learn high-quality representations from unlabeled images, thereby improving policy learning [36].

For each encoder, BYOL uses two neural networks, Fig. 3: 1) an online network parameterized by  $\phi$  that consists of an encoder ( $f_{s,\phi}, f_{g,\phi}$ ), a projector ( $g_{s,\phi}, g_{g,\phi}$ ), and a predictor ( $q_{s,\phi}, q_{g,\phi}$ ); and 2) a target network parameterized by  $\xi$  that consists of an encoder ( $f_{s,\xi}, f_{g,\xi}$ ), and a projector ( $g_{s,\xi}, g_{g,\xi}$ ). Herein, we represent these parameters in general as ( $f_\phi, g_\phi, q_\phi, f_\xi, g_\xi$ ) as the training of  $f_s$  and  $f_g$  follow the same procedure. The online network and the target network share the same architecture for the encoder and the projector. The projector and the predictor are represented by a multiple-layer perceptron (MLP). The weights of the target network are an exponential moving average of the online network weights.

Two distributions of image augmentations including random resizing, cropping, color jittering were applied to obtain two augmented views  $v$  and  $v'$  from the input observation image  $o$ . The online network takes  $v$  as input, and outputs representation  $y_\phi = f_\phi(v)$ , projection  $z_\phi = g_\phi(y_\phi)$ , and a prediction  $q_\phi(z_\phi)$ . The target network takes as input  $v'$ , and outputs representation  $y'_\xi = f_\xi(v')$  and projection  $z'_\xi = g_\xi(y'_\xi)$ . The loss function is defined as the mean squared error (MSE) between the normalized online prediction and target projection:

$$\mathcal{L}_{\phi,\xi} = \left\| \frac{q_\phi(z_\phi)}{\|q_\phi(z_\phi)\|_2} - \frac{z'_\xi}{\|z'_\xi\|_2} \right\|_2^2. \quad (5)$$

BYOL uses a symmetrical loss by swapping  $v$  and  $v'$  as input to the online and target networks again to compute  $\tilde{\mathcal{L}}_{\phi,\xi}$ :

$$\mathcal{L}_{\phi,\xi}^{\text{BYOL}} = \mathcal{L}_{\phi,\xi} + \tilde{\mathcal{L}}_{\phi,\xi}. \quad (6)$$

The final BYOL loss is the summation of the loss for  $f_s$ ,  $\mathcal{L}_{s,\phi,\xi}^{\text{BYOL}}$  and the loss for  $f_g$ ,  $\mathcal{L}_{g,\phi,\xi}^{\text{BYOL}}$ :

$$\mathcal{L}^{\text{BYOL}} = \mathcal{L}_{s,\phi,\xi}^{\text{BYOL}} + \mathcal{L}_{g,\phi,\xi}^{\text{BYOL}}. \quad (7)$$

To ensure that the static encoder learns only the static features from the environment, we modified the standard

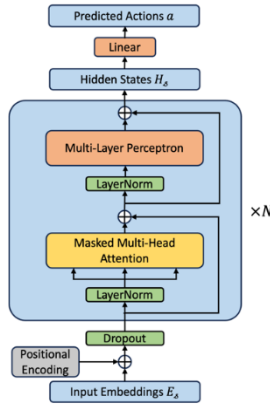


Fig. 4. Structure of the Navigation Network.

BYOL procedure [35] by generating the two augmented views  $(v, v')$  from two different images  $(o^s, o^d)$  of the same view of the scene.  $o^d$  denotes an RGB image that contains dynamic obstacles (i.e., other robots) while  $o^s$  denotes an image that contains only static obstacles. Therefore, the static encoder learns only the common static obstacle features shared between the images  $(o^s, o^d)$ . For the general encoder, we follow the standard BYOL procedure [35] and generate two different augmented views from the same image  $o^d$ .

### C. Navigation Network

The Navigation Network is used to generate the robot's action  $a_{t+1}$  given the sequence of embeddings  $E_{s,t}$ . Our Navigation Network uses a causal transformer model based on the Generative Pre-trained Transformer 2 (GPT-2) [37]. We use a causal transformer model as its self-attention mechanism can effectively utilize sequential memory of past embeddings, enabling the network to reason about the spatial layout of the environment based on the robot trajectory.

The structure of our Navigation Network, Fig. 4, consists of three stacked transformer blocks, and a linear layer. To enhance the model's ability to understand the temporal and multi-modal nature of the input data, positional encodings are introduced as learnable embeddings for each timestep and each modality, which are added to the input embedding sequence  $E_{s,t}$ .

Dropout is applied to the  $E_s$  to prevent overfitting [38].  $E_s$  is then sent into  $N = 3$  stacked transformer blocks, each consisting of a masked multi-head attention (MMHA) submodule and a MLP submodule. The context length of each transformer block (maximum number of input embeddings) is 1024. In the MMHA submodule, the embeddings  $E_s$  are linearly projected into  $h = 2$  heads of keys  $K$ , queries  $Q$  and values  $V$  in the dimension of  $d_k = 64$  for the computation of self-attention. The MMHA submodule is connected to a MLP that has a hidden layer and residual connection. The last transformer block outputs a sequence of hidden states  $H_s$ :

$$H_s = (h_g, h_{R,1}, h_{o,1}^s, h_{o,1}^{ca}, \dots, h_{R,t}, h_{o,t}^s, h_{o,t}^{ca}). \quad (8)$$

We concatenate the target hidden state  $h_g$  with the observation hidden state  $h_{o,i}^{ca}$  and provide the concatenated hidden state  $[h_g; h_{o,i}^{ca}]$  into a linear layer to predict the next navigation action  $\hat{a}_i$ . This hidden state concatenation aims to

help the causal transformer model implicitly detect the target, thus leading to an improved navigation policy.

### 1) Training Loss

We utilize the Decision Transformer [39] offline RL method for training the Navigation Network. Offline RL is used as online RL methods are sample inefficient in tasks with sparse rewards such as robot navigation [40]. The loss of the Navigation Network is computed using the MSE between the predicted actions  $\hat{a}_i$  and ground-truth actions  $a_i$ :

$$\mathcal{L}^{DT} = \frac{1}{T} \sum_{t=1}^T \|a_t - \hat{a}_t\|^2. \quad (9)$$

## V. DATASET COLLECTION

We collected three datasets in simulated environments to train NavFormer: 1) Robot Exploration Dataset,  $\mathcal{D}_e$ , 2) Collision Avoidance Dataset,  $\mathcal{D}_{ca}$ , and 3) Representation Learning Dataset,  $\mathcal{D}_{ssl}$ . These datasets were collected in 3D simulated environments from mobile robots (Jackal robots from Clearpath) using the Robot Operating System (ROS) and Gazebo, Fig. 1. The target objects were represented with different geometric shapes (sphere, box) and colors (green, red, white, yellow, blue).

**Exploration Dataset  $\mathcal{D}_e$ :** This dataset comprises 3,496 robot trajectories and the corresponding target RGB images, totaling 342,954 timesteps for a single robot exploration task in 3D environment with only static obstacles (i.e., walls). Each robot trajectory was obtained in a different environment with a random size ranging from  $5 \times 5$  m to  $17.5 \times 17.5$  m. The trajectory  $\tau$  consists of returns-to-go  $\hat{R}$ , observations  $o$ , and actions  $a$ . To generate this dataset, the Frontier Exploration method in [41] was used to select the nearest frontier location for the robot. The robot planned a global path using A\* [42] and followed this path using DWA [22] as the local planner.  $\hat{R}_1$  is initialized to be 1. The robot receives a positive reward of 1 when it has successfully navigated to the target.  $\mathcal{D}_e$  is used to train NavFormer to learn the skill of exploration.

**Collision Avoidance Dataset  $\mathcal{D}_{ca}$ :** This dataset comprises 7,467 robot trajectories and the corresponding target images, totaling 469,378 timesteps for the task of multi-robot collision avoidance in dynamic environments. Each trajectory was obtained in a  $12.5 \times 12.5$  m environment with the number of dynamic obstacles ranging from 2 to 8. NH-ORCA [20] was used to generate the robot trajectories. Target location was set as the navigation goal for the robot.  $\hat{R}_1$  was defined as above. This dataset was used to learn the skill of collision avoidance.

**Representation Learning Dataset  $\mathcal{D}_{ssl}$ :** This dataset consists of 98,000 image pairs captured in 3D mazes containing dynamic obstacles. It was collected in 1,000 different randomly generated environments with sizes ranging from  $5 \times 5$  m to  $17.5 \times 17.5$  m and the number of dynamic obstacles ranging from 4 to 25. Each image pair contained two RGB images  $(o_i^s, o_i^d)$  taken by the robot's onboard camera. To collect this dataset: 1) we randomly placed all dynamic obstacles in different locations, and recorded their observations (i.e.,  $o_i^d$ ) and locations; and 2) a single robot was placed at all previous locations and its own observations were captured (i.e.,  $o_i^s$ ). We aligned each  $o_i^s$  with its corresponding  $o_i^d$  based on the



locations where  $o_t^s$  and  $o_t^d$  were taken. This dataset was used for the representation learning of the dual-visual encoders.

## VI. TRAINING

We used a cross-task training approach for the policy learning of NavFormer. Namely, we decomposed the robot TDN task into the two sub-tasks of: 1) single robot exploration, and 2) multi-robot collision avoidance. NavFormer was trained on  $\mathcal{D}_e$  and  $\mathcal{D}_{ca}$  to learn exploration and collision avoidance skills. To compute  $\mathcal{L}^{DT}(9)$ , we alternated between  $\mathcal{D}_e$  and  $\mathcal{D}_{ca}$  during each training iteration to sample trajectories. To train the dual-visual encoders, we use  $\mathcal{D}_{ssl}$  to sample image pairs to compute  $\mathcal{L}^{BYOL}$ , (7). The final loss is:

$$\mathcal{L} = \mathcal{L}^{BYOL} + \mathcal{L}^{DT}. \quad (10)$$

Training was performed on a Ubuntu20.04 workstation with an RTX3070 GPU, an AMD Ryzen Threadripper 3960X CPU and 128GB of memory. The training of the dual-visual encoders utilized a batch size of 512. The Adam optimizer [43] was used for weight optimization of BYOL with a learning rate of 0.0004 and weight decay of 0.0004. NavFormer was trained utilizing a batch size of 25 for trajectory sampling from  $\mathcal{D}_e$  and a batch size of 150 for trajectory sampling from  $\mathcal{D}_{ca}$ . We used different batch sizes for trajectory sampling to balance the total number of frames in each batch as trajectories in  $\mathcal{D}_e$  were longer than trajectories in  $\mathcal{D}_{ca}$ . Dropout is applied to the causal transformer with zero-out probability of 0.1. The AdamW optimizer [44] was used to train the NavFormer with a learning rate of 0.0002 and weight decay of 0.0001, over a span of 10,000 iterations.

## VII. SIMULATED EXPERIMENTS

We conducted two sets of experiments to evaluate the overall performance of our NavFormer architecture, we: 1) conducted a comparison study with our approach and state-of-the-art (SOTA) learning methods to compare TDN strategies, and 2) performed an ablation study to investigate the contributions of the design choices on the training and architecture of NavFormer.

### A. Comparison Study Experiments

We used two performance metrics for these experiments: 1) mean success rate (SR) of robots reaching target objects, and 2) Success weighted by normalized inverse Path Length (SPL) which measures the efficiency of the navigation method [45]:

$$\text{SPL} = \frac{1}{N_t} \sum_{i=1}^{N_t} S_i \frac{\ell_i}{\max(\mathcal{P}_i, \ell_i)}, \quad (11)$$

where  $N_t$  denotes the number of robot trials,  $S_i$  is a binary indicator of success in trial  $i$ .  $\ell_i$  denotes the shortest path length from the start location of the robot to the target location, and  $\mathcal{P}_i$  denotes the actual robot path length.

We randomly generated a total of 54 new unseen 3D environments in Gazebo consisting of static obstacles, target objects, and dynamic obstacles (robots). The sizes of these environments were  $7.5 \times 7.5$  m,  $12.5 \times 12.5$  m, and  $17.5 \times 17.5$  m, Fig. 5. Each robot had a different target object to navigate to. The target objects were randomly generated with different geometric shapes and colors, and locations. We deployed 2, 4 and 6 robots in each environment.

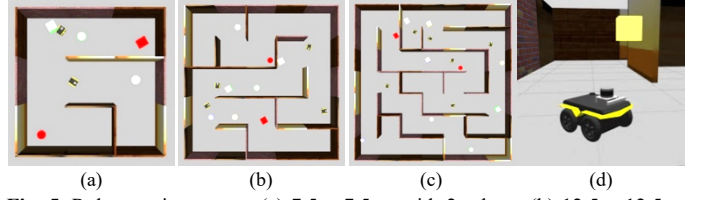


**Fig. 5.** Robot environments: (a)  $7.5 \times 7.5$  m with 2 robots, (b)  $12.5 \times 12.5$  m with 4 robots, (c)  $17.5 \times 17.5$  m with 6 robots, and (d) a mobile robot and a target object.

1) *Comparison Methods*: We benchmarked our NavFormer method against the following learning-based SOTA methods:

**Deep Siamese Actor-Critic (DSAC)** [9]: The Deep Siamese Actor-Critic model uses Resnet-50 [14] for the Siamese layers to extract visual features from observations and target images and FCLs for the scene-specific layers to generate navigation actions. DSAC is selected as its Siamese layers can implicitly detect target objects by fusing features from observation and target images for the TDN task.

**Memory-Augmented Target-Driven Navigation (MA-TDN)** [6]: MA-TDN uses an attention module to retrieve the memory of past robot observations and combines the retrieved memory embeddings with the current observation and target image embeddings to generate navigation actions. MA-TDN is selected as it accounts for past memory of observations for spatial reasoning.

**Decision Transformer (DT)** [39]: The decision transformer uses only one visual encoder for feature extraction from visual observations. The navigation action is generated using the hidden state of the observation embedding. DT is selected as it is conditioned on multi-modal robot historical trajectory for navigation decision making.

For both DSAC and MA-TDN, we convert their discrete action space to continuous space by outputting a mean and variance to define a Gaussian distribution for action sampling. Training of DSAC and MA-TDN were achieved with PPO [28]. DT was trained on  $\mathcal{D}_e$  and  $\mathcal{D}_{ca}$  using Eq. (9).

2) *Experimental Procedure*: At the beginning of each trial, robots were both randomly located in the environment and randomly assigned an RGB image of a target  $g$ . Each robot found its target while the other robots were treated as dynamic obstacles. A robot found a target when the distance between the target and robot was within 1.5m. A trial terminated when either all robots found their corresponding targets or the total timesteps exceeded 500. Each timestep is 0.2s. A new environment was randomly generated every 10 trials.

3) *Results*: The SR and SPL results for NavFormer and the SOTA methods across the different environment sizes and number of robots are presented in Table I. In general, NavFormer consistently outperformed DSAC, MA-TDN and DT. As the environment size increased, SR and SPL decreased for all methods due to the: 1) increased level of difficulty introduced by more static obstacles in the larger environments, and 2) longer travel distance between start and target location with the allocated time. DSAC achieved the lowest SR for all robot conditions in the large-sized environment, with also the lowest SPL for 2 and 6 robots for this environment. For the small and medium-sized environments, it had the lowest SR for at least 2 robot conditions. This is due to DSAC making

TABLE I  
COMPARISON BETWEEN NAVFORMER AND SOTA METHODS

Setup		DSAC		MA-TDN		DT		NavFormer (ours)	
Environment size (m)	# of robots	SR	SPL	SR	SPL	SR	SPL	SR	SPL
7.5 × 7.5	2	53.33%	0.377	61.67%	0.315	57.50%	0.419	80.83%	0.562
	4	47.08%	0.353	46.67%	0.248	47.92%	0.395	66.25%	0.465
	6	42.78%	0.337	43.06%	0.234	40.28%	0.332	54.44%	0.435
12.5 × 12.5	2	24.17%	0.179	30.00%	0.159	39.17%	0.258	53.33%	0.374
	4	19.17%	0.133	23.33%	0.137	26.25%	0.201	48.89%	0.378
	6	23.89%	0.180	23.06%	0.118	31.94%	0.231	48.75%	0.359
17.5 × 17.5	2	10.00%	0.084	20.83%	0.117	34.17%	0.222	44.17%	0.316
	4	10.00%	0.085	13.75%	0.078	22.08%	0.151	38.33%	0.279
	6	10.56%	0.092	16.39%	0.098	22.50%	0.169	35.56%	0.272

navigation decisions solely based on its current observation without incorporating temporal information such as past observations to reason about the spatial layout of an unknown environment. Consequently, DSAC resulted in redundant coverage, and therefore, was not able to reach target objects within the time limit. Unlike DSAC, MA-TDN incorporated temporal information by retrieving past observations via attention mechanism. However, MA-TDN had the lowest SPL for the small-sized environments as it treated dynamic obstacles as static. This resulted in inaccurate representation of the spatial layouts of the environments, and lead to redundant coverage. DT compared with DSAC and MA-TDN had higher SR and SPL in the medium and large-sized environments, regardless of the number of robots. This was due to DT learning the navigation policy directly from expert demonstrations (i.e.,  $\mathcal{D}_e$  and  $\mathcal{D}_{ca}$ ). As DT is an offline RL method it does not suffer from sample inefficiency and suboptimal policies as online methods such as DSAC and MA-TDN can [40].

NavFormer had the highest SR and SPL scores across all the three environments and number of robots. NavFormer was able to achieve accurate spatial layout representation from invariant features extracted by the static encoder, minimizing the need for redundant coverage of an environment. Target hidden state concatenation enabled NavFormer to achieve improved implicit target detection during navigation by directly conditioning on the target hidden states. This aids the robot to recognize and reach the target object when it is within robot’s camera view, thereby facilitating task completion.

A Friedman test was performed for the two metrics across all four methods. The results showed a statistically significant difference ( $p < 0.001$ ) for both SR and SPL. Post-hoc Wilcoxon Signed-rank tests with Bonferroni correction were conducted between NavFormer and each comparison method. The results showed NavFormer had statistically significant higher SR and SPL than the SOTA methods ( $p < 0.0167$ ).

### B. Ablation Study

We conducted an ablation study to investigate the impact of the design choices on the training methods and architecture design of NavFormer. Namely, we considered:

- 1) **NavFormer without SSL:** This variant was trained using only the loss of  $\mathcal{L}^{DT}$ , Eq. (9). This is used to investigate the influence of SSL in learning both static and general features from visual observations.
- 2) **NavFormer without Training on  $\tau^e$ :** For this variant, when computing  $\mathcal{L}^{DT}$ , Eq. (9), robot exploration trajectories  $\tau^e$  from

TABLE II  
ABLATION STUDY

Methods	SR	SPL
NavFormer	48.75%	0.359
NavFormer w/o SSL	39.58%	0.272
NavFormer w/o Target Hidden States Concatenation	32.08%	0.261
NavFormer w/o $\tau^e$	12.08%	0.109
NavFormer w/o $\tau^{ca}$	40.83%	0.256

$\mathcal{D}_e$  are not included. This is to investigate the importance of exploration skills learned from cross-task training.

3) **NavFormer without Training on  $\tau^{ca}$ :** For this variant, when computing  $\mathcal{L}^{DT}$ , Eq. (9), robot collision avoidance trajectories  $\tau^{ca}$  from  $\mathcal{D}_{ca}$  are not included. This is to investigate the importance of collision avoidance skills learned from cross-task training in NavFormer.

4) **NavFormer without Target Hidden States Concatenation:** For this variant, the feed-forward layer of Navigation Network includes input only from the hidden state of the observation  $h_{o,t}^{ca}$  to generate  $\hat{a}_t$ . This is to investigate the target hidden state concatenation influence on detecting the target object during navigation.

In total, we conducted 60 trials in 6 environments of  $12.5 \times 12.5$  m with 4 robots. A new environment is randomly generated every 10 trials.

1) *Results:* The results of the ablation study are presented in Table II. NavFormer achieved the highest SR and SPL among all variants. NavFormer without training on  $\tau^e$  achieved the lowest SR and SPL, indicating that exploration skill contributed the most to the increased performance of NavFormer. However, we found that NavFormer without training on  $\tau^{ca}$  achieved the highest SR and SPL for all variants. We postulate that this is due to two reasons: 1) exploration skills are more important than the dynamic obstacle avoidance skills for the completion of the TDN task in unknown and dynamic environments; and 2) NavFormer inherently acquires collision avoidance with static obstacles skills during the learning of exploration skills from  $\tau^e$ , diminishing the incremental benefit of learning from dynamic obstacle avoidance trajectories  $\tau^{ca}$ . A Friedman test was conducted for the metrics of SR and SPL across all variants. A statistically significance difference ( $p < 0.001$ ) was found for each metric. Post-hoc analysis using Wilcoxon Signed-rank tests with Bonferroni correction showed a statistical difference between NavFormer and each variant ( $p < 0.0125$ ).

## VIII. CONCLUSION

In this paper, we present the development of a novel end-to-end DL model, NavFormer, to address the challenging problem

of robot target-driven navigation in unknown and dynamic environments. Our approach uniquely combines a Dual-Visual Encoder system with a transformer-based Navigation Network. The former is trained via self-supervised learning, while the latter uses offline reinforcement learning. We transfer both learned exploration and collision avoidance skills to a robot to achieve target-driven navigation without the need for fine-tuning. Extensive simulated experiments were conducted with varying environment sizes and different number of dynamic obstacles. The results show that NavFormer outperformed state-of-the-art learning-based methods in successfully navigating to targets. An ablation study validated our design choices for NavFormer architecture and training method. Future work will expand our architecture by incorporating object recognition backbones for common objects and different dynamic obstacles in everyday environments.

## REFERENCES

- [1] Y. Liu and G. Nejat, "Multirobot Cooperative Learning for Semiautonomous Control in Urban Search and Rescue Applications," *J. Field Robot.*, vol. 33, no. 4, pp. 512–536, 2016.
- [2] A. H. Tan, F. P. Bejarano, Y. Zhu, R. Ren, and G. Nejat, "Deep Reinforcement Learning for Decentralized Multi-Robot Exploration With Macro Actions," *IEEE Robot. Autom. Lett.*, vol. 8, no. 1, pp. 272–279, Jan. 2023.
- [3] A. Fung, B. Benhabib, and G. Nejat, "Robots Autonomously Detecting People: A Multimodal Deep Contrastive Learning Method Robust to Intraclass Variations," *IEEE Robot. Autom. Lett.*, vol. 8, no. 6, pp. 3550–3557, Jun. 2023.
- [4] R. R. Murphy, "Activities of the rescue robots at the World Trade Center from 11-21 september 2001," *IEEE Robot. Autom. Mag.*, vol. 11, no. 3, pp. 50–61, Sep. 2004.
- [5] A. H. Reddy, B. Kalyan, and Ch. S. N. Murthy, "Mine Rescue Robot System – A Review," *Procedia Earth Planet. Sci.*, vol. 11, pp. 457–462, 2015.
- [6] L. Mezghan *et al.*, "Memory-Augmented Reinforcement Learning for Image-Goal Navigation," in *Proc. IEEE Int. Conf. Intell. Robots Syst.*, 2022, pp. 3316–3323.
- [7] P. Fiorini and Z. Shiller, "Motion planning in dynamic environments using velocity obstacles," *Int. J. Robot. Res.*, vol. 17, no. 7, pp. 760–772, Jul. 1998.
- [8] C. Yu *et al.*, "DS-SLAM: A Semantic Visual SLAM towards Dynamic Environments," in *Proc. IEEE Int. Conf. Intell. Robot Syst.*, 2018, pp. 1168–1174.
- [9] Y. Zhu *et al.*, "Target-driven visual navigation in indoor scenes using deep reinforcement learning," in *Proc. IEEE Int. Conf. Robot. Autom.*, 2017, pp. 3357–3364.
- [10] A. Devo, G. Mezzetti, G. Costante, M. L. Fravolini, and P. Valigi, "Towards Generalization in Target-Driven Visual Navigation by Using Deep Reinforcement Learning," *IEEE Trans. Robot.*, vol. 36, no. 5, pp. 1546–1561, Oct. 2020.
- [11] Q. Wu, X. Gong, K. Xu, D. Manocha, J. Dong, and J. Wang, "Towards Target-Driven Visual Navigation in Indoor Scenes via Generative Imitation Learning," *IEEE Robot. Autom. Lett.*, vol. 6, no. 1, pp. 175–182, Jan. 2021.
- [12] A. Vaswani *et al.*, "Attention is all you need," *Adv. Neural Inf. Process. Syst.*, pp. 5999–6009, 2017.
- [13] E. Wijmans *et al.*, "DD-PPO: Learning Near-Perfect PointGoal Navigators from 2.5 Billion Frames," 2019, *arXiv:1911.00357*.
- [14] K. He, X. Zhang, S. Ren, and J. Sun, "Deep Residual Learning for Image Recognition," in *Proc. IEEE Conf. Comput. Vis. Pattern Recognit.*, 2016, pp. 770–778.
- [15] V. Mnih *et al.*, "Asynchronous Methods for Deep Reinforcement Learning," in *Proc. Int. Conf. Mach. Learn.*, 2016, vol. 48, pp. 1928–1937.
- [16] S. Hochreiter and J. Schmidhuber, "Long Short-Term Memory," *Neural Comput.*, vol. 9, no. 8, pp. 1735–1780, Nov. 1997.
- [17] L. Espeholt *et al.*, "IMPALA: Scalable Distributed Deep-RL with Importance Weighted Actor-Learner Architectures," in *Proc. Int. Conf. Mach. Learn.*, Jul. 2018, pp. 1407–1416.
- [18] J. Tobin, R. Fong, A. Ray, J. Schneider, W. Zaremba, and P. Abbeel, "Domain randomization for transferring deep neural networks from simulation to the real world," in *Proc. IEEE Int. Conf. Intell. Robots Syst.*, Dec. 2017, pp. 23–30.
- [19] J. D. Van Berg, M. Lin, and D. Manocha, "Reciprocal velocity obstacles for real-time multi-agent navigation," in *Proc. IEEE Int. Conf. Robot. Automat.*, 2008, pp. 1928–1935.
- [20] J. Alonso-Mora, A. Breitenmoser, M. Rufli, P. Beardsley, and R. Siegwart, "Optimal reciprocal collision avoidance for multiple non-holonomic robots," in *Distrib. Auton. Robot. Syst.*, Springer, 2013, pp. 203–216.
- [21] O. Khatib, "Real-Time Obstacle Avoidance for Manipulators and Mobile Robots," *Int. J. Robot. Res.*, vol. 5, no. 1, pp. 90–98, Mar. 1986.
- [22] D. Fox, W. Burgard, and S. Thrun, "The dynamic window approach to collision avoidance," *IEEE Robot. Autom. Mag.*, vol. 4, no. 1, pp. 23–33, 1997.
- [23] P. Long, T. Fanl, X. Liao, W. Liu, H. Zhang, and J. Pan, "Towards optimally decentralized multi-robot collision avoidance via deep reinforcement learning," in *Proc. IEEE Int. Conf. Robot. and Automat.*, 2018, pp. 6252–6259.
- [24] J. Zeng, R. Ju, L. Qin, Y. Hu, Q. Yin, and C. Hu, "Navigation in Unknown Dynamic Environments Based on Deep Reinforcement Learning," *Sensors*, vol. 19, no. 18, Jan. 2019.
- [25] R. Han *et al.*, "Reinforcement Learned Distributed Multi-Robot Navigation With Reciprocal Velocity Obstacle Shaped Rewards," *IEEE Robot. Autom. Lett.*, vol. 7, no. 3, pp. 5896–5903, Jul. 2022.
- [26] M. Everett, Y. F. Chen, and J. P. How, "Motion Planning among Dynamic, Decision-Making Agents with Deep Reinforcement Learning," in *Proc. IEEE Int. Conf. Intell. Robots Syst.*, Dec. 2018, pp. 3052–3059.
- [27] G. Sartoretti *et al.*, "PRIMAL: Pathfinding via Reinforcement and Imitation Multi-Agent Learning," *IEEE Robot. Autom. Lett.*, vol. 4, no. 3, pp. 2378–2385, 2019.
- [28] J. Schulman, F. Wolski, P. Dhariwal, A. Radford, and O. Klimov, "Proximal Policy Optimization Algorithms," pp. 1–12, 2017.
- [29] K. Cho *et al.*, "Learning Phrase Representations using RNN Encoder-Decoder for Statistical Machine Translation," 2014, *arXiv:1406.1078*.
- [30] M. Babaeizadeh, I. Frosio, S. Tyree, J. Clemons, and J. Kautz, "Reinforcement Learning through Asynchronous Advantage Actor-Critic on a GPU," 2017, *arXiv:1611.06256*.
- [31] W. Khaksar, S. Vivekananthan, K. S. M. Saharia, M. Yousefi, and F. B. Ismail, "A review on mobile robots motion path planning in unknown environments," *Proc. IEEE Int. Symp. Robot. Intell. Sens.*, pp. 295–300, Apr. 2016.
- [32] F. A. Oliehoek and C. Amato, *A Concise Introduction to Decentralized POMDPs*, vol. 1. Cham: Springer, 2016.
- [33] S. Nasiriany, V. H. Pong, S. Lin, and S. Levine, "Planning with Goal-Conditioned Policies," 2019, *arXiv:1911.08453*.
- [34] V. Mnih *et al.*, "Human-level control through deep reinforcement learning," *Nature*, vol. 518, no. 7540, pp. 529–533, 2015.
- [35] J.-B. Grill *et al.*, "Bootstrap Your Own Latent - A New Approach to Self-Supervised Learning," 2020, *arXiv:2006.07733*.
- [36] M. Laskin, A. Srinivas, and P. Abbeel, "CURL: Contrastive Unsupervised Representations for Reinforcement Learning," 2020, *arXiv:2004.04136*.
- [37] A. Radford, J. Wu, R. Child, D. Luan, D. Amodei, and I. Sutskever, "Language Models are Unsupervised Multitask Learners," *OpenAI blog*, 2019.
- [38] N. Srivastava, G. Hinton, A. Krizhevsky, I. Sutskever, and R. Salakhutdinov, "Dropout: A simple way to prevent neural networks from overfitting," *J. Mach. Learn. Res.*, vol. 15, no. 1, pp. 1929–1958, 2014.
- [39] L. Chen *et al.*, "Decision Transformer: Reinforcement Learning via Sequence Modeling," 2021, *arXiv:2106.01345*.
- [40] R. S. Sutton and A. G. Barto, *Reinforcement learning: an introduction*, Second edition. in *Adaptive Comput. Mach. Learn. Ser.*, Cambridge, Massachusetts: The MIT Press, 2018.
- [41] B. Yamauchi, "Frontier-based approach for autonomous exploration," in *Proc. IEEE Int. Symp. Comput. Intell. Robot. Automat.*, 1997, pp. 146–151.
- [42] P. Hart, N. Nilsson, and B. Raphael, "A Formal Basis for the Heuristic Determination of Minimum Cost Paths," *IEEE Trans. Syst. Sci. Cybern.*, vol. 4, no. 2, pp. 100–107, 1968.
- [43] D. P. Kingma and J. Lei, "Adam: A Method for Stochastic Optimization," 2015, *arXiv:1412.6980*.
- [44] I. Loshchilov and F. Hutter, "Decoupled Weight Decay Regularization," 2019, *arXiv:1711.05101*.
- [45] P. Anderson *et al.*, "On Evaluation of Embodied Navigation Agents," 2018, *arXiv:1807.06757*.